ASM | Journal of Bacteriology

Check for updates

Rv3400 is a phosphoglucomutase required for trehalose metabolism in *Mycobacterium tuberculosis*

Yi Liu,[1] Nadine Ruecker,[2] Valwynne Faulkner,[3] Kavitha Rachineni,[4] Nada Al-Saffar,[4] Elisabeth Oskoui,[1] Larissa Zarate Garcia,[5] Jessica Emma Rowley,[5] Pablo Villacampa Teixeira,[1] Tiago R. D. Costa,[1] Eachan Johnson,[3] Brian D. Robertson,[6] Sabine Ehrt,[2] Gerald Larrouy-Maumus[1]

AUTHOR AFFILIATIONS See affiliation list on p. 11.

ABSTRACT *Mycobacterium tuberculosis* (Mtb) causes over 1 million deaths from tuberculosis (TB) every year and remains a major burden on human health. Reducing the deadly impact of TB requires a better understanding of the strategies used by *M. tuberculosis* to adapt its metabolism, survive, and persist in the human host. Previous enzymological studies reported that the Mtb *rv3400* gene encodes a β-phosphoglucomutase; however, its role in *M. tuberculosis* metabolism had not been investigated. Here, we show that deletion of *rv3400* causes a 30-fold increase in β-D-glucose-1-phosphate, confirming its primary function as a β-phosphoglucomutase. Deletion of *rv3400* also causes a growth defect when trehalose is the sole carbon source. Targeted metabolomics revealed that metabolites associated with redox homeostasis, including ergothioneine, mycothiol, and mycothione, are decreased in the Mtb Δ*rv3400* strain compared with the wild type, indicating altered tolerance to redox stress. Consistent with this, the Δ*rv3400* strain showed increased susceptibility to oxidative stress induced by H_2O_2 and cumene hydroperoxide, conditions that Mtb encounters during infection. This work advances our understanding of trehalose metabolism in Mtb and suggests that Rv3400 may represent a target for the development of new antimicrobial therapies.

IMPORTANCE Trehalose metabolism plays a cornerstone role in *Mycobacterium tuberculosis* physiology and virulence. A better understanding of the metabolism of this essential disaccharide is therefore required to develop new strategies to eradicate tuberculosis. Here, we characterize *M. tuberculosis* lacking the β-phosphoglucomutase encoded by *rv3400*. We show that deletion of *rv3400* leads to accumulation of β-D-glucose-1-phosphate, impaired growth when trehalose is used as the sole carbon source, and increased susceptibility to oxidative stress. Taken together, these data provide evidence that Rv3400 is required for optimal catabolism of trehalose.

KEYWORDS metabolomics, trehalose, *Mycobacterium tuberculosis*, glycolysis, enzyme

Mycobacterium tuberculosis (Mtb) causes over 1 million deaths annually and remains a major global health threat (1). Although antibiotics have been used for decades, drug resistance and persistent infections severely limit current treatments against this global killer. A key challenge in combating Mtb is understanding how it adapts to host environments, such as macrophages, by reprogramming its metabolism and gene expression. Addressing this knowledge gap is important for identifying new druggable targets and achieving the WHO's tuberculosis eradication goals through next-generation therapeutics.

Recent *in vitro* studies have characterized Rv3400 as a β-phosphoglucomutase (β-PGM), an enzyme that catalyzes the isomerization of β-D-glucose-1-phosphate (G1P) to β-D-glucose-6-phosphate (G6P) via a β-D-glucose-1,6-bisphosphate (β-G1,6-bisP)

Editor Patricia A. Champion, University of Notre Dame, Notre Dame, Indiana, USA

Address correspondence to Gerald Larrouy-Maumus, g.larrouy-maumus@imperial.ac.uk.

The authors declare no conflict of interest.

See the funding table on p. 12.

Received 24 June 2026
Accepted 3 August 2026
Published 3 September 2026

Copyright © 2026 Liu et al. This is an open-access article distributed under the terms of the Creative Commons Attribution 4.0 International license.

Downloaded from https://journals.asm.org/journal/jb on 28 September 2026 by 2a0c:5bc0:40:1008:de4a:3eff:fe6a:56ad.

Downloaded from https://journals.asm.org/journal/jb on 28 September 2026 by 2a0c:5bc0:40:1008:de4a:3eff:fe6a:56ad.

intermediate (2) (Fig. 1). The enzyme is closely linked to central carbon metabolism, as G6P serves as a key metabolic node to produce ATP and NADPH via glycolysis and the pentose phosphate pathway, respectively (3). Although Rv3400 is dispensable for *in vitro* growth of Mtb H37Rv (4–6), it is required for bacterial growth in the spleen of C57BL/6J mice (5, 6). Furthermore, using genetic interaction mapping, Joshi et al. reported the interaction between Rv3400 and the virulence-associated mycobacterial cell entry 4 (*mce4*) operon, suggesting a potential role in Mtb virulence (7).

Recent studies also suggest that Rv3400 could be part of the trehalose degradation pathway (2) (Fig. 1). Trehalose is a non-reducing disaccharide (1-O-α-D-glucopyranosyl-α-D-glucopyranoside) found in insects, plants, and microbial cells. In mycobacteria, trehalose is constitutively present in cells grown in standard laboratory media and is the only free sugar readily detectable in the cytoplasm, comprising approximately 1.5%–3% of the total cellular dry weight (8). Trehalose has well-established protective functions during cryopreservation and desiccation and is known to enhance microbial survival under environmental stress *in vivo*. In mycobacteria, trehalose is not only a reserved energy source but also an active player in metabolic pathways, as suggested by the dynamic turnover of the trehalose pool found in the rapid-growing mycobacteria *Mycobacterium smegmatis* (9). It is also incorporated into many mycobacterial glycolipids, including cord factor (trehalose 6,6′-dimycolate), sulfolipids (acylated trehalose-2′-sulfate derivatives), and trehalose-containing lipooligosaccharides (10–12). These multiple roles further underscore the importance of trehalose metabolism in Mtb survival and pathogenesis.

Here, we investigated the impact of *rv3400* deletion on Mtb metabolism. We found that the Mtb Δ*rv3400* strain has a growth defect when trehalose is used as the carbon source and accumulates β-D-glucose-1-phosphate, consistent with the loss of β-PGM activity. We further show that *rv3400* deletion alters carbon metabolism and redox metabolites, leading to increased susceptibility to oxidative stress.

RESULTS AND DISCUSSION

Deletion of *rv3400* leads to an increase in β-D-glucose-1-phosphate level

Recent work has identified Rv3400 as a β-PGM *in vitro* (2). To confirm its enzymatic function, we constructed the *rv3400* deletion mutant (Δ*rv3400*), complemented (Δ*rv3400*::*rv3400*), and catalytic site mutant (Δ*rv3400*::*rv3400*$_{D29A}$) strains and measured their growth in carbon-defined liquid medium. As shown in Fig. 2A, compared to the wild-type strain, deletion of *rv3400* did not impair growth when glucose was used as the sole carbon source. To further validate the role of Rv3400 as a β-PGM,

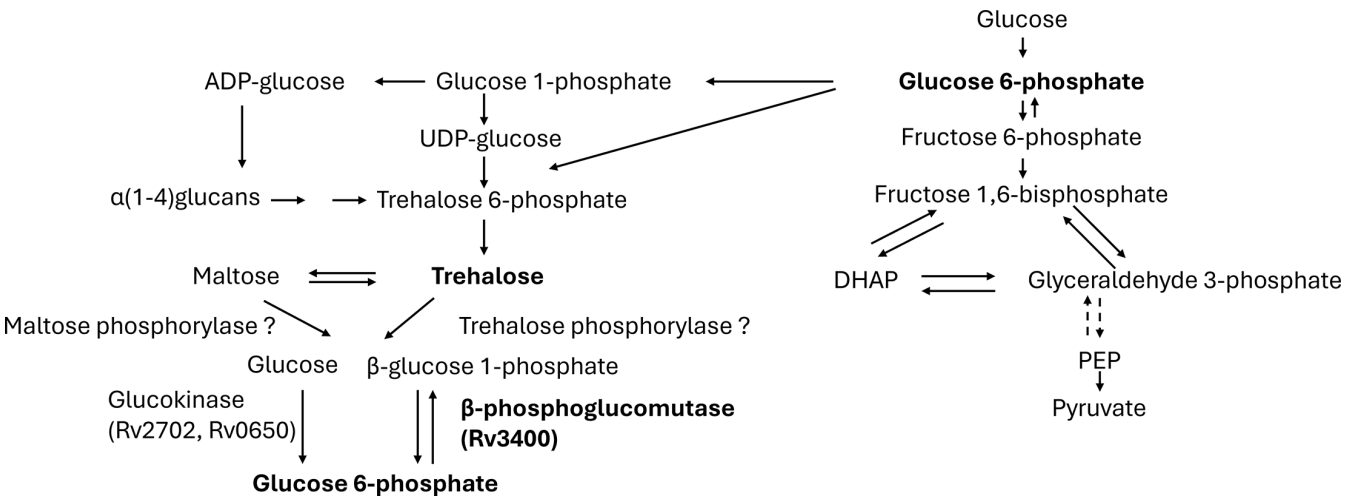


FIG 1 Scheme presenting the trehalose metabolism pathway.

Downloaded from https://journals.asm.org/journal/jb on 28 September 2026 by 2a0c:5bc0:40:1008:de4a:3eff:fe6a:56ad.

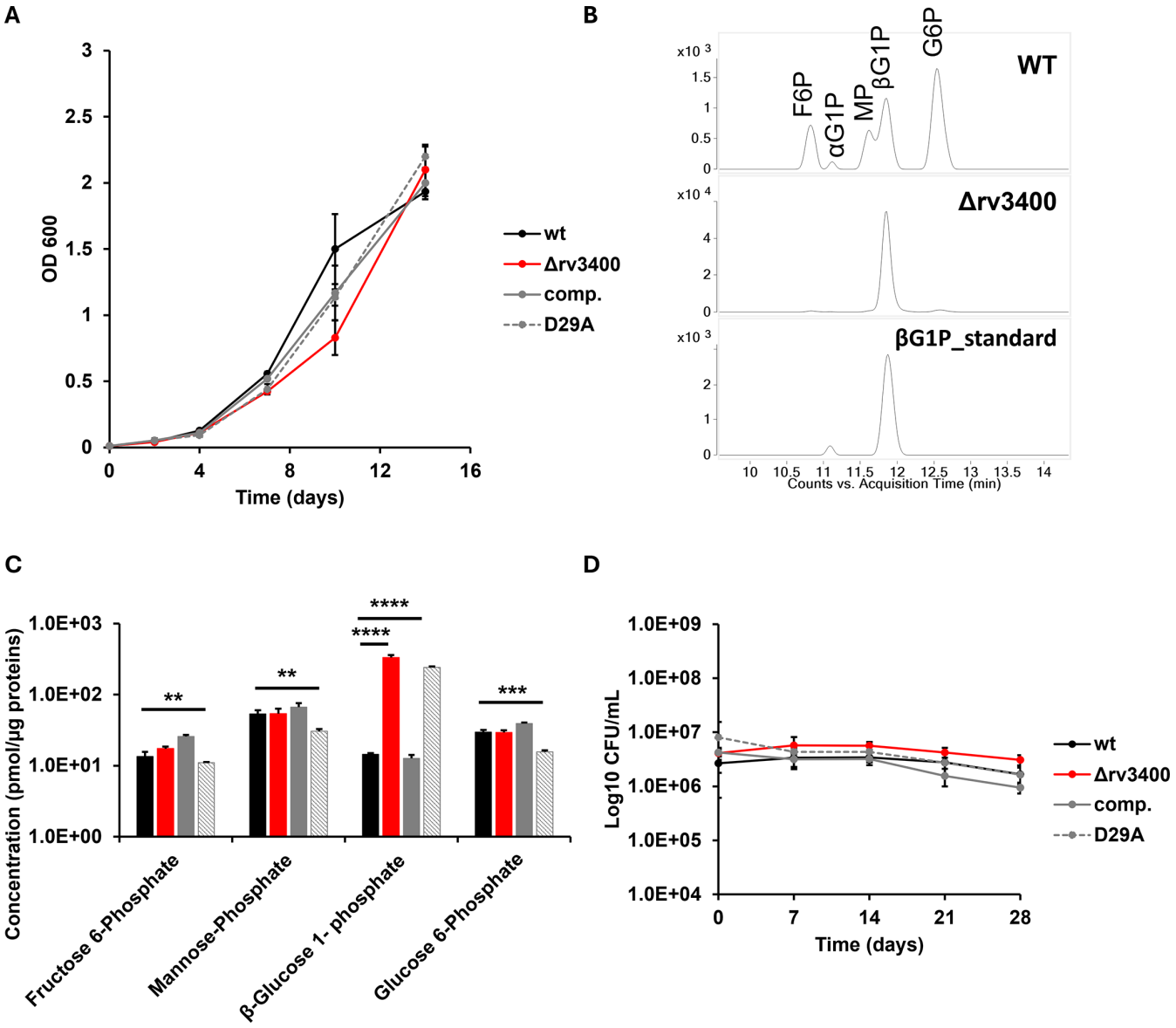


FIG 2 Rv3400 is a phosphoglucomutase in *Mycobacterium tuberculosis*. (A) Growth curves of wild-type (black) and Δ*rv3400* (red) strains with glucose as the sole carbon source. (B) Extraction ion chromatograms for ions at *m/z* 259.024 $[M–H]^-$ for the wild-type (top), Δ*rv3400* strains (middle), and β-D-glucose-1-phosphate standard (bottom). (C) Bar charts displaying the concentration in pmol/µg proteins for the five relevant phosphorylated sugars (F6P: fructose-6-phosphate; G1P: glucose-1-phosphate; βG1P: β-D-glucose-1-phosphate; MP: mannose-6-phosphate/mannose-1-phosphate; and G6P: glucose-6-phosphate). Wild type: black bars, Δ*rv3400*: red bars, complemented: gray bars, and D29A: shaded gray bars. (D) Survival assay under PBS starvation as measured by the number of viable cells (CFU/mL). Asterisks indicate levels of significance compared to wild-type strain bacteria. The significance level of differences was determined by unpaired Student's *t*-tests, with *, $P < 0.05$; **, $P < 0.01$; ***, $P < 0.001$; ****, $P < 0.0001$.

we used liquid chromatography-mass spectrometry (LC-MS) analysis to extract the ion chromatograms for the ion at *m/z* 259.024 $[M–H]^-$, assigned to monosaccharide phosphates: fructose 6-phosphate (retention time [RT], 11.1 min), glucose-1-phosphate (RT, 11.3 min), mannose-1-phosphate/mannose-6-phosphate (RT, 11.6 min), β-glucose-1-phosphate (RT, 11.8 min), and glucose-6-phosphate (RT, 12.4 min). In the Δ*rv3400* strain, the peak corresponding to β-D-glucose-1-phosphate (RT, 11.8 min) increased (Fig. 2B). The assignment of this peak to β-D-glucose-1-phosphate was confirmed by nuclear magnetic resonance (NMR) (Supplemental text and Fig. S1 to S6). In addition, quantification of the four monosaccharide phosphates revealed that *rv3400* deletion

specifically elevated the concentration of β-glucose-1-phosphate (Fig. 2C), confirming that Rv3400 is a β-PGM involved in the conversion of β-D-glucose-1-phosphate into β-D-glucose-6-phosphate. Interestingly, the levels of the four other monosaccharide phosphates—fructose 6-phosphate, mannose 1-phosphate/6-phosphate, and glucose 6-phosphate—were not altered in the Δ*rv3400* compared to the wild type (Fig. 2C).

To gain further insights into how the Δ*rv3400* maintains monosaccharide phosphate levels similar to those of the wild type, we performed qRT-PCR on the two glucokinase genes *rv2702* and *rv0650*. As shown in Table S1, no significant differences were observed between the wild type and Δ*rv3400* as well as Δ*rv3400*::*rv3400*$_{D29A}$. To investigate this observation further, we performed stable isotope labeling using [U-$^{13}C_6$]-glucose. This experiment tested whether carbon metabolism differed in Δ*rv3400* compared to the wild type. As shown in Table S2, no changes in the ^{13}C incorporation were observed for either fructose 6-phosphate or glucose 6-phosphate. However, ^{13}C incorporation into β-glucose-1-phosphate was markedly decreased in Δ*rv3400* and Δ*rv3400*::*rv3400*$_{D29A}$ compared to the wild type, with approximately ~25% compared to ~60%, respectively.

Together, these experiments indicate that deletion of *rv3400* impairs the conversion of β-D-glucose-1-phosphate into glucose 6-phosphate (Fig. 1) without affecting the levels of the other monosaccharide phosphates, as the turnover of both fructose 6-phosphate and glucose 6-phosphate was not altered by *rv3400* deletion.

Because glucose phosphorylation is not essential for long-term PBS starvation (13), we next investigated the effect of prolonged PBS starvation on the survival of the Mtb Δ*rv3400* strain. As shown in Fig. 2D, Rv3400 was not required for bacterial viability during starvation, consistent with previous literature (13). Measurement of reactive oxygen species (ROS) after 28 days of PBS starvation using CellROX Deep Red showed no difference in ROS production between the wild-type and Δ*rv3400* strain (Fig. S6), confirming that Rv3400 is dispensable under long-term PBS starvation.

Deletion of *rv3400* impairs growth when trehalose is used as the sole carbon source

The trehalose recycling pathway mediated by the LpqY-SugA-SugB-SugC ATP-binding cassette transporter is critical during acute Mtb infection in the mouse model, when exponential replication occurs and trehalose can serve as a carbon source; disruption of this pathway may cause starvation in nutrient-limited *in vivo* microenvironments (14, 15). Given the proposed role of Rv3400 in trehalose recycling, we assessed the growth of Δ*rv3400* and Δ*rv3400*::*rv3400*$_{D29A}$ strains with trehalose as the sole carbon source. As shown in Fig. 3A, both strains exhibited growth defects under this condition.

To further support this observation, we performed growth curves using 0.05%, 0.02%, and 0.4% glucose or trehalose. As expected, glucose was used as the sole carbon source, and increasing glucose concentration increased the growth of the wild-type, Δ*rv3400,* and complemented strains. However, when trehalose was used as the sole carbon source, growth increased with higher trehalose concentrations in the wild-type and complemented strains, whereas no increase in growth was observed for Δ*rv3400* when more carbon was available in the culture medium (Fig. S7). To rule out contaminants that could interfere with bacterial growth, such as fatty acids originating from bovine serum albumin (BSA) fraction V, we repeated the experiment using fatty-acid-free BSA fraction V. A similar result was observed: the Δ*rv3400* strain did not display increased growth with increasing trehalose concentration (Fig. S8).

Targeted metabolomics further revealed that the Δ*rv3400* mutant accumulated a 30-fold higher β-glucose-1-phosphate pool, while showing twofold, twofold, and threefold reductions in fructose 6-phosphate, mannose 1-phosphate/6-phosphate, and glucose 6-phosphate pools, respectively (Fig. 3B). A similar trend is observed in the metabolic profile of the D29A strain (Fig. 3B). Taken together, these data demonstrate that Rv3400 is required for optimal use of trehalose in Mtb.

Because bacterial growth represents only one aspect of bacterial metabolism, we next performed LC-MS metabolomics analysis of the intracellular metabolome of each

Downloaded from https://journals.asm.org/journal/jb on 28 September 2026 by 2a0c:5bc0:40:1008:de4a:3eff:fe6a:56ad.

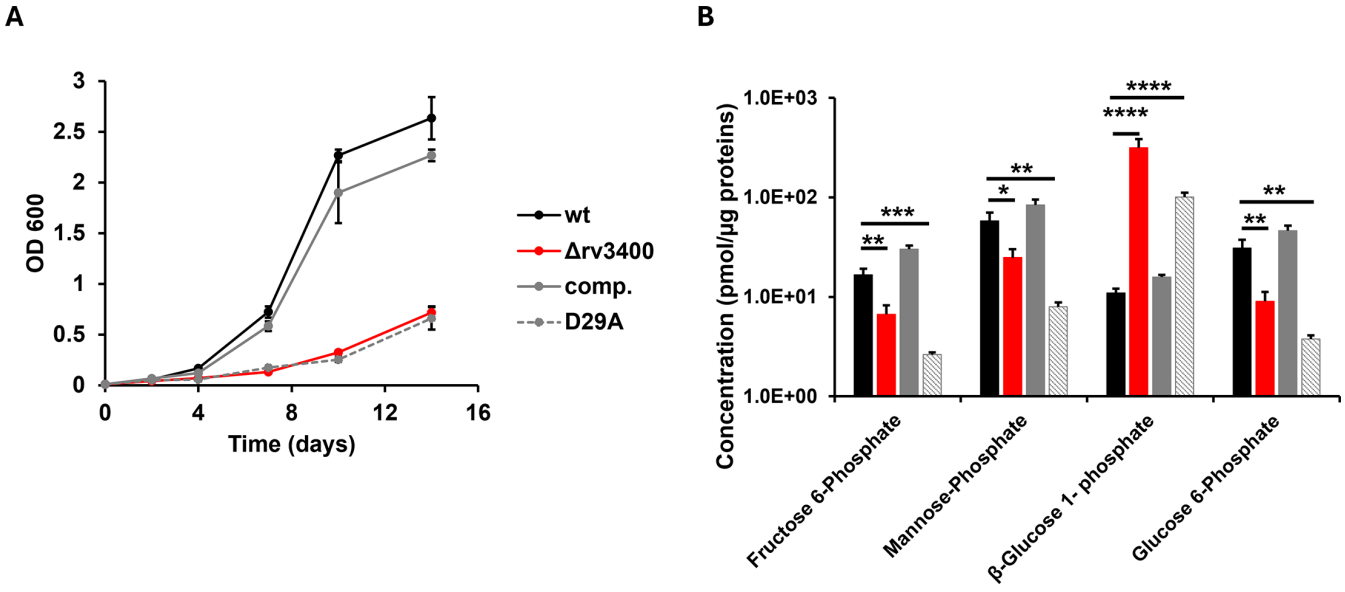


FIG 3 Rv3400 is required for trehalose recycling. (A) Growth curves of wild-type (black), Δ*rv3400* (red), complemented (gray), and D29A (dashed gray) strains with trehalose as the sole carbon source. (B) Bar charts displaying the concentration in pmol/µg proteins for the four relevant phosphorylated sugars (F6P: fructose-6-phosphate; βG1P: β-D-glucose-1-phosphate; MP: mannose-6-phosphate/mannose-1-phosphate; and G6P: glucose-6-phosphate). Wild type: black bars, Δ*rv3400*: red bars, complemented: gray bars, and D29A: shaded gray bars.The significance levels of difference were determined by unpaired Student's t-tests, with *, $P < 0.05$; **, $P < 0.01$; ***, $P < 0.001$; ****, $P < 0.0001$.

strain. We selected a set of 36 metabolites belonging to central carbon metabolism, the tricarboxylic acid cycle, amino acid metabolism, nucleotide metabolism, redox metabolism, and peptidoglycan metabolism (Table S3).

Consistent with the observation that *rv3400* deletion does not strongly affect the global metabolome when glucose is used as the sole carbon source, the volcano plot identified only one significantly increased metabolite, β-glucose-1-phosphate, in the Δ*rv3400* mutant strain compared with the wild type (Fig. 4A).

However, when trehalose was used as the sole carbon source, 12 of the 36 metabolites showed significant changes in the Δ*rv3400* mutant strain compared to the wild type (Fig. 4B). Notably, the redox metabolites ergothioneine and mycothione showed some of the largest decreases in the Δ*rv3400* mutant. Using targeted LC-MS metabolomics, we measured the intracellular levels of mycothiol (MSH), mycothione (MSSM), a metabolite crucial for maintaining intracellular redox homeostasis in mycobacterial cells (16), and ergothioneine, a sulfur-containing histidine derivative with potent antioxidant and redox-buffering properties (17–20), in the wild-type, Δ*rv3400*, and complemented strains. No changes in MSH, MSSM, or ergothioneine levels were observed when the wild-type, Δ*rv3400,* and complemented strains were grown on glucose as the sole carbon source (Fig. 4C). By contrast, when grown on trehalose as the sole carbon source, the Δ*rv3400* strain showed an approximately threefold decrease in both MSH and MSSM and an approximately 10-fold decrease in ergothioneine compared with the wild type (Fig. 4D). These results indicate that Rv3400-dependent trehalose metabolism is important for maintaining bacterial redox homeostasis.

Rv3400 is required to maintain redox balance when trehalose is used as the sole carbon source

Based on the metabolomics data (Fig. 4D), which showed that MSH, MSSM, and ergothioneine levels were decreased in the Δ*rv3400* mutant grown on trehalose as the sole carbon source, we hypothesized that this strain would have compromised redox balance. To test this hypothesis, we first investigated the viability of the wild-type, Δ*rv3400,* and complemented strains after 24 h exposure to reductive stress

Downloaded from https://journals.asm.org/journal/jb on 28 September 2026 by 2a0c:5bc0:40:1008:de4a:3eff:fe6a:56ad.

Downloaded from https://journals.asm.org/journal/jb on 28 September 2026 by 2a0c:5bc0:40:1008:de4a:3eff:fe6a:56ad.

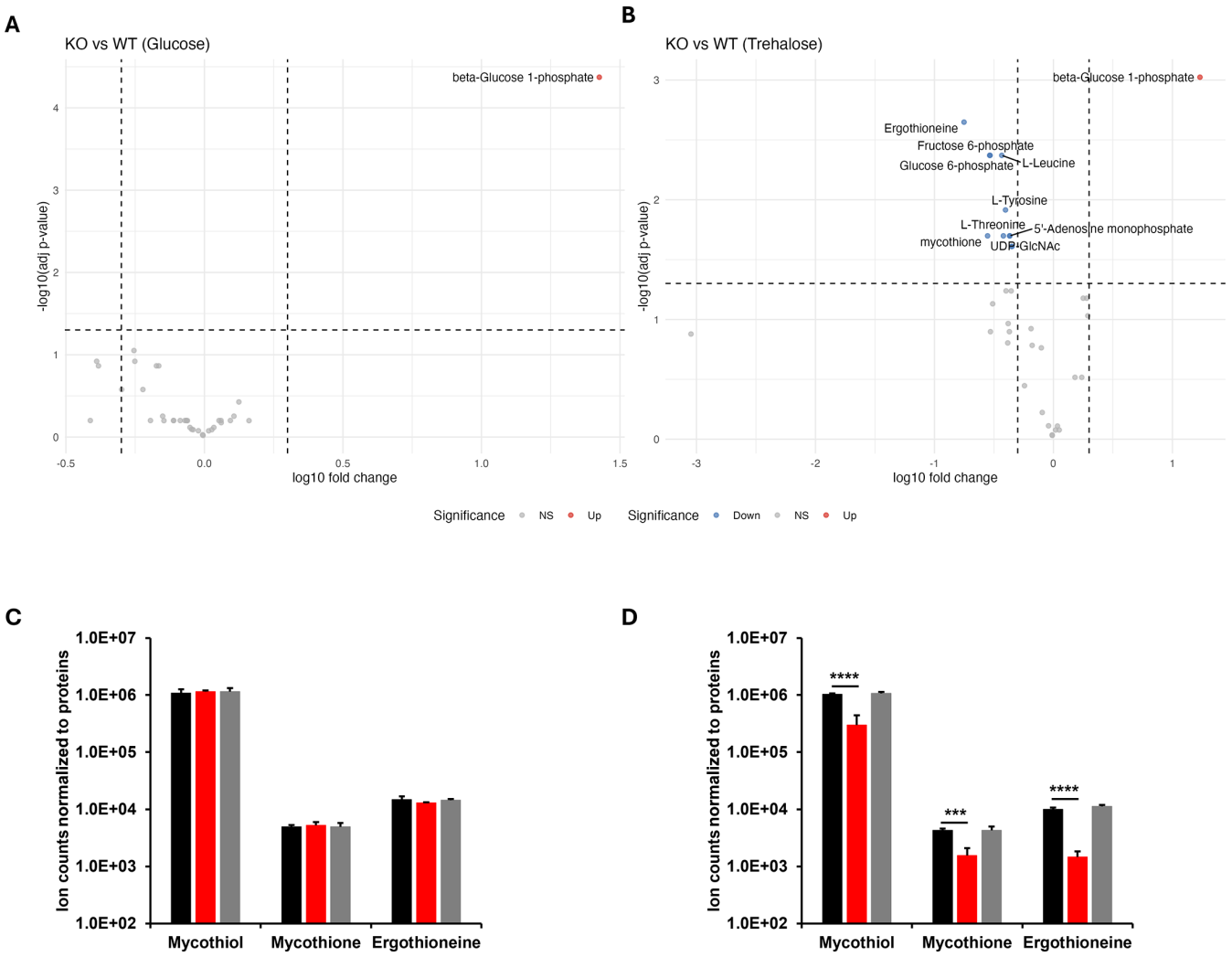


FIG 4 Deletion of *rv3400* impairs the biosynthesis of redox metabolites. (A) Volcano plots of targeted metabolites for strains grown in glucose as the sole carbon source. (B) Volcano plots of targeted metabolites for strains grown in trehalose as the sole carbon source. (C) MSH, MSSM, and ergothioneine levels for the wild-type (black), Δ*rv3400* (red), and complemented (gray) strains when using glucose as the sole carbon source. (D) MSH, MSSM, and ergothioneine levels for the wild-type (black), Δ*rv3400* (red), and complemented (gray) strains when using trehalose as the sole carbon source. Asterisks indicate levels of significance compared to wild-type strain bacteria. The significance level of differences was determined by unpaired Student's *t*-tests, with *, $P < 0.05$; **, $P < 0.01$; ***, $P < 0.001$; ****, $P < 0.0001$. Volcano plots display log10 fold change against −log10(adjusted p-value), with thresholds indicated by dashed lines, and the most significant metabolites were annotated based on adjusted *p*-values.

(dithiothreitol, DTT) or oxidative stress (cumene hydroperoxide, CHP) using either glucose or trehalose as the sole carbon source. When grown in glucose as the sole carbon source, no changes in CFU/mL were observed across strains exposed to DTT (Fig. 5A). Exposure to CHP caused an approximately 1 $\log_{10}$ decrease in viable bacteria in the wild-type strain and an approximately 2 $\log_{10}$ decrease in the Δ*rv3400* strain, suggesting that *rv3400* deletion renders bacteria more susceptible to oxidative stress. When grown in trehalose as the sole carbon source (Fig. 5B), exposure to DTT led to an approximately 0.3 $\log_{10}$ reduction in viable bacteria in the wild-type strain, whereas no change in CFU was observed in the Δ*rv3400* strain. Following CHP treatment, an approximately 1 $\log_{10}$ decrease in viable bacteria was observed in the wild-type strain, and an approximately 3 $\log_{10}$ decrease was observed in the Δ*rv3400* strain. A similar phenotype was observed using H_2O_2 as a more physiological *in vitro* oxidative stressor. Although no changes in CFU were observed when glucose was used as the sole carbon source, the Δ*rv3400* strain showed an approximately 1 $\log_{10}$ decrease in CFU compared with the wild type when

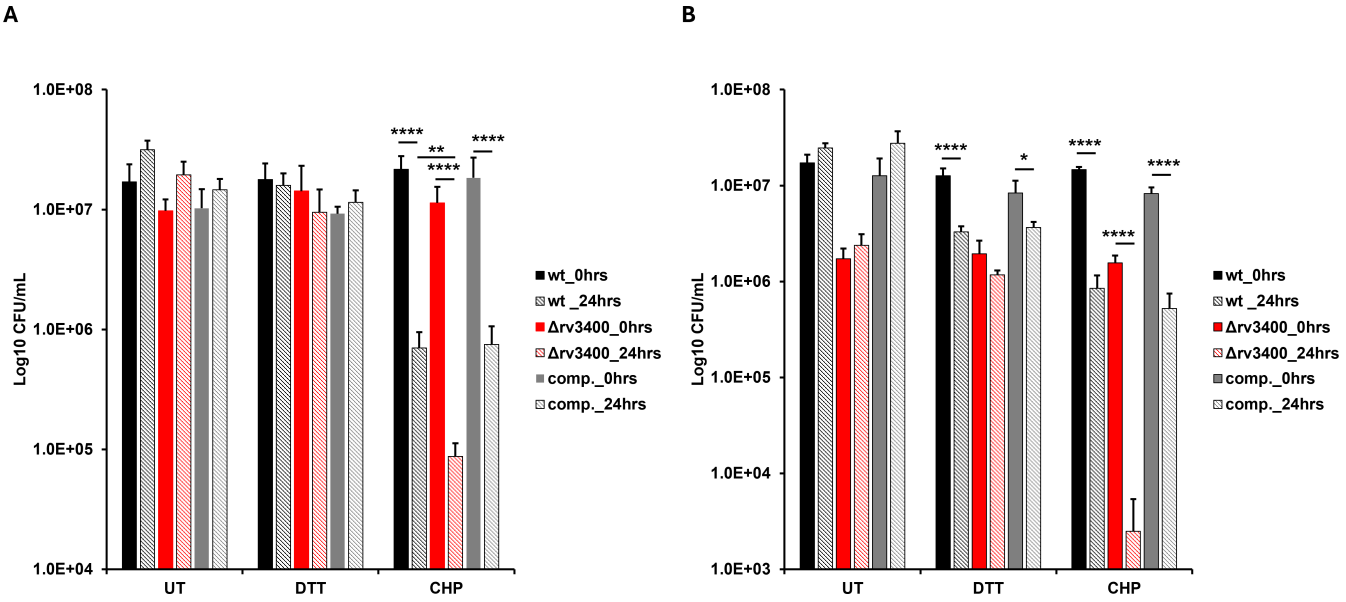


FIG 5 Deletion of *rv3400* leads to an increase in susceptibility to oxidative stress. (A) Bar charts displaying the number of viable bacteria expressed as CFU/mL for the wild type: black bars, Δ*rv3400*: red bars, complemented: gray bars at time 0 h for untreated (UT), DTT, or CHP-treated bacteria, and for the wild type: dashed black bars, Δ*rv3400*: dashed red bars, complemented: dashed gray bars at time 24 h for UT, DTT, or CHP-treated bacteria, when using glucose as the sole carbon source. (B) Bar charts displaying the number of viable bacteria expressed as CFU/mL for the wild type: black bars, Δ*rv3400*: red bars, complemented: gray bars at time 0 h for UT, DTT, or CHP-treated bacteria, and for the wild type: dashed black bars, Δ*rv3400*: dashed red bars, complemented: dashed gray bars at time 24 h for UT, DTT, or CHP-treated bacteria, when using trehalose as the sole carbon source. Asterisks indicate levels of significance. The significance levels of differences were determined by unpaired Student's *t*-tests, with *, $P < 0.05$; **, $P < 0.01$; ***, $P < 0.001$; ****, $P < 0.0001$.

trehalose was used as the sole carbon source (Fig. S9), confirming that the Δ*rv3400* strain is more susceptible to oxidative stress than the wild type.

Taken together, our data demonstrate that Rv3400 is a β-PGM required for optimal trehalose utilization when trehalose is present as the sole carbon source. This study provides in-cell validation of Rv3400 function in Mtb trehalose metabolism and highlights its contribution to bacterial redox homeostasis. The trehalose synthesis and recycling pathway has been studied for its involvement not only in Mtb regrowth but also in the formation of persisters and the development of multidrug resistance (21, 22). Therefore, our study on Rv3400 contributes substantially to understanding this pathway as an important part of Mtb metabolism.

MATERIALS AND METHODS

Bacterial strains and growth conditions

The Mtb Δ*rv3400* mutant was constructed in strain H37Rv by allelic exchange using a recombineering approach as previously described (23).

A pMV306 plasmid with the *rv3400* native promoter was used as the backbone for construction of the *rv3400* complementation plasmid. To generate a complementation of *rv3400* under its native promoter, the integrating expression vector pMV306 KanR (24) was digested with EcoRV-HF (NEB) and subsequently column purified using the QIAquick purification kit (Qiagen). DNA fragments comprising the full length of *rv3400* and *rv3400* D29A along with 150 bp upstream of the annotated start codon were synthesized (GenScript). The synthesized fragments included 20 bp overhangs at both the 5′ and 3′ ends homologous to the digested vector. NEBuilder HiFi DNA assembly (NEB) was used to ligate the linearized vector and synthesized inserts. Correct assembly of the recombinant plasmids was confirmed by Nanopore sequencing.

Downloaded from https://journals.asm.org/journal/jb on 28 September 2026 by 2a0c:5bc0:40:1008:de4a:3eff:fe6a:56ad.

Precultures of all strains were grown in 30 mL square bottles containing 10 mL 7H9 medium (DIFCO) supplemented with 0.2% wt/vol glucose, 0.5% wt/vol standard BSA, 0.08% wt/vol NaCl, 0.05% wt/vol tyloxapol, and appropriate antibiotics. The bottles were incubated in a shaking incubator at 37°C and 120 rpm. 7H10 agar plates (Sigma) were supplemented with 0.2% wt/vol glycerol, 0.2% wt/vol dextrose, 0.5% wt/vol BSA, and 0.08% wt/vol NaCl for growth on solid medium in a 37°C static incubator. For carbon source concentration dependence, fatty-acid-free BSA fraction V was used, while carbon source concentrations were either 0, 0.05%, 0.2%, or 0.4% final concentration wt/vol.

Growth curves

Growth curve assays were performed in a 30 mL square bottles (Nalgene) containing 10 mL pre-warmed 7H9 (DIFCO) medium. Precultures of bacteria were grown and used to inoculate these flasks at OD_{600nm} = 0.01. Inoculated flasks were incubated in a 37°C static incubator, and OD_{600nm} measurements were taken at least five times to produce growth curves until the stationary phase.

Bacteria viability under starvation

To quantify the number of viable cells under PBS starvation, mid-log phase cultures were spun down, washed twice with PBS, and resuspended at an OD_{600nm} = 0.1 in PBS 0.5% tyloxapol. Cultures were sampled on days 0, 7, 14, 21, and 28 and plated on 7H10 agar plates. Colonies were counted after 3–4 weeks of incubation at 37°C.

Bacteria viability under redox stresses

To quantify the number of viable cells under redox stresses, mid-log phase cultures were exposed to 10 mM DTT, 400 µM CHP, for 24 h or 10 mM H_2O_2 for 1 h. Cultures were sampled at day 0 and 24 h after exposure for DTT and CHP, and after 1 h for H_2O_2 and plated on 7H10 agar plates. Colonies were counted after 3–4 weeks of incubation at 37°C.

Metabolite extraction

Mtb strains were grown in 10 mL flasks with 7H9 medium to reach OD_{600nm} of approximately 0.8. After incubation, bacteria were collected by centrifugation at 3,000 × *g*, 4°C for 10 min. Pellets were washed once with cold sterile PBS and metabolically quenched in extraction solution (40% acetonitrile, 40% methanol, and 20% ddH_2O). Samples were transferred to microtubes containing 0.1 mm acid-washed zirconia beads and lysed using a FastPrep-24 homogenizer twice at 6.0 m/s for 30 s, with a 5 min interval. Supernatants were transferred to 0.22 µm spin X column filters (Costar) and filtered twice by centrifuging at 15,000 × *g* for 30 min. The bacterial biomass of the individual samples was determined by measuring the residual protein content of the metabolite extracts using the BCA assay kit (Thermo) (25, 26). After filtration, the flowthrough was mixed with an equal volume of acetonitrile and centrifuged at 15,000 × *g* for 10 min. A total of 100 µL of the mixture was loaded into polypropylene snap vials (Agilent Technologies) for LC-MS analysis.

Metabolite extraction with stable isotope (^{13}C) labeling

[U-$^{13}C_6$] glucose was purchased from Cambridge Isotope Laboratories, UK. ^{13}C-labeled 7H9 medium was prepared by substituting dextrose in the supplement with [U-$^{13}C_6$] glucose at the same concentration. Mtb strains were grown in 10 mL flasks with 7H9 medium to reach OD_{600nm} of approximately 0.6–0.8. On the day of labeling, bacteria were collected by centrifugation and resuspended in 5 mL ^{13}C-labeled 7H9. Labeled cultures were incubated in a shaking incubator at 37°C for 4 h to allow label incorporation. After incubation, bacteria were collected by centrifugation at 3,000 × *g* for 10 min at 4°C. Pellets were washed once with cold sterile PBS and metabolically quenched in extraction solution (40% acetonitrile, 40% methanol, and 20% ddH_2O). Samples were

Downloaded from https://journals.asm.org/journal/jb on 28 September 2026 by 2a0c:5bc0:40:1008:de4a:3eff:fe6a:56ad.

transferred to microtubes containing 0.1 mm acid-washed zirconia beads and lysed using a FastPrep-24 homogenizer twice at 6.0 m/s for 30 s, with a 5 min interval. Supernatants were transferred to 0.22 µm spin X column filters (Costar) and filtered twice by centrifuging at 15,000 × *g* for 30 min. After filtration, the flowthrough was mixed with an equal volume of acetonitrile and centrifuged at 15,000 × *g* for 10 min. A total of 100 µL of the mixture was loaded into polypropylene snap vials (Agilent Technologies) for LC-MS analysis.

LC-MS

The data were acquired with an Agilent 1290 Infinity II UHPLC coupled to a 6545 LC/Q-TOF system. Chromatographic separation was performed with an Agilent InfinityLab Poroshell 120 HILIC-Z (2.1 × 100 mm, 2.7 µm [p/n 675775-924]) column. The HILIC-Z methodology was optimized for polar acidic metabolites. The column compartment was set at 50°C. For easy and consistent mobile-phase preparation, a concentrated 10× solution consisting of 100 mM ammonium acetate (pH 9.0) in water was prepared to produce mobile phases A and B. Mobile phase A consisted of 10 mM ammonium acetate in water (pH 9) with a 5 µM Agilent InfinityLab deactivator additive (p/n 5191-4506), and mobile phase B consisted of 10 mM ammonium acetate (pH 9) in 10:90 (vol:vol) water/acetonitrile with 5 µM Agilent InfinityLab deactivator additive (p/n 5191-4506). The following gradient was applied at a flow rate of 0.25 mL/min: 0 min, 96% B; 2 min, 96% B; 5.5 min, 88% B; 8.5 min, 88% B; 9 min, 86% B; 14 min, 86% B; 17 min, 82% B; 23 min, 65% B; 24 min, 65% B; 24.5 min, 96% B; 26 min, 96% B, and 3 min of re-equilibration at 96% B. Accurate MS was performed using an Agilent Accurate Mass 6545 QTOF apparatus. Dynamic mass axis calibration was achieved by continuous infusion after the chromatography of a reference mass solution using an isocratic pump connected to an electrospray ionization source operated in negative-ion mode. The following parameters were used: gas temperature, 225°C; drying gas, 13 L/min^{-1}; sheath gas temperature, 350°C; nebulizer pressure, 35 psi; sheath gas flow, 12 L/min^{-1}; capillary voltage, 3,500 V; nozzle voltage, 0 V; fragmentor voltage, 125 V; skimmer 45 V, and octupole 1 RF voltage, 750 V. The data were collected in centroid 4 GHz (extended dynamic range) mode.

LC-MS metabolomics data analysis

MassHunter Qualitative Analysis software was used to check the extracted ion chromatograms of the *m/z* values of interest and obtain their retention times, which were used to construct the personal compound database and library (PCDL) for following analysis. Standards were purchased from Sigma-Aldrich: α-D-fructose-6-phosphate (F1502-1G), α-D-glucose-6-phosphate (G7250), α-D-glucose-1-phosphate (G7000-5G), Calbiochem α-D-mannose-6-phosphate (444100-50MG), and Biosynth Ltd. for β-D-glucose-1-phosphate (MG02984).

Metabolite data were processed in MetaboAnalyst (v6.0) and R (v4.5.2) using a custom analysis pipeline. Technical replicates were collapsed by averaging values within each biological replicate.

Metabolite matrices (metabolites × samples) were constructed for differential analysis data sets. Batch effects attributable to biological repeat were corrected using the ComBat function (sva package v3.58.0), with a design matrix including genetic background and carbon source as covariates to preserve biological signal.

For differential metabolite analysis (volcano plots), linear models were fitted using limma (v3.66.0) on batch-corrected, $\log_{10}$-transformed data. Limma fits a linear model to each metabolite and applies empirical Bayes moderation, which improves variance estimation by borrowing information across metabolites and shrinking individual variance estimates toward a common value. Analyses were performed separately for each carbon source, comparing knockout and wild-type strains.

Differential abundance was reported as $\log_{10}$ fold change ($\log_{10}$FC), consistent with the $\log_{10}$ transformation applied to the data. *P* values were adjusted using the Benjamini–Hochberg false discovery rate (FDR). Metabolites were considered significant if the

Downloaded from https://journals.asm.org/journal/jb on 28 September 2026 by 2a0c:5bc0:40:1008:de4a:3eff:fe6a:56ad.

FDR-adjusted *P* value was <0.05 and absolute $\log_{10}$FC was >0.3. Volcano plots display $\log_{10}$ fold change against $-\log_{10}$(adjusted *P* value), with thresholds indicated by dashed lines, and the most significant metabolites were annotated based on adjusted *P* values.

Stable isotope labeling

Under the experimental conditions described above using [U-$^{13}C_6$]-glucose (99%), the extent of ^{13}C labeling of each metabolite was determined by dividing the summed peak-height ion intensities of all ^{13}C-labeled species by the ion intensity of both labeled and unlabeled species using Agilent Profinder version B.8.0.00 service pack 3.

NMR

Dried extracts of wild-type and knockout bacterial cells were resuspended in 200 µL of a mixture of 90% D_2O (Sigma-Aldrich) and 10% phosphate buffer (pH 7.4) prepared for NMR analysis as reported in Dona et al. (27). The solution was vortexed for 1 min before centrifugation at 17,000 × *g* for 10 min at 4°C. An aliquot of 180 µL of the supernatant was transferred into a 3 mm NMR tube for NMR analysis.

All NMR spectra were acquired using a Bruker Avance III console combined with a 14.1 T magnet (600 MHz for ^1H NMR). The system was equipped with a 5 mm broadband inverse probe with *z*-axis magnetic field-gradient and a Bruker Sample Jet system, set to 3 mm shuttle mode with a cooling rack maintaining refrigerated tubes at 6°C.

A pre-saturated proton 1D-NOESY pulse sequence was used to obtain 1D ^1H NMR spectra, with the offset set at 4.70 ppm for water suppression. A total of 65,536 data points were collected with a spectral width of 20.0 ppm and a total of 64 scans (27).

A set of 2D NMR experiments was conducted for structural elucidation of the unknown compound present in the knockout samples, including Jres (J-resolved spectroscopy), ^1H–^1H COSY (correlation spectroscopy), and ^1H–^1H TOCSY (total correlation spectroscopy). All NMR data were processed using TopSpin 3.6 (Bruker BioSpin GmbH, Rheinstetten, Germany). Processing steps included Fourier transformation, phasing, baseline correction, and spectral calibration.

Spiking experiments using an authentic chemical standard were used to further confirm that the unknown compound in the knockout sample was β-D-glucose-1-phosphate. The NMR sample of the knockout cells was spiked with increasing volumes of β-D-glucose-1-phosphate chemical standard (Biosynth Ltd; MG02984) ranging from 0.5 µL to 2 µL, prepared at a concentration of 30 µM in D_2O, resulting in an increase in the signal intensity of the NMR resonances of interest in the knockout sample.

ROS measurement using CellROX Deep Red

Cultures after 28 days of starvation in PBS containing 0.5% tyloxapol were harvested by centrifugation (3,000 × *g* for 5 min) and resuspended in 200 µL PBS containing 5 µM CellROX Deep Red (catalog no. C10422; Invitrogen) and incubated at 37°C for 30 min. After incubation, cells were washed to remove residual dye by centrifugation (3,000 × *g* for 5 min). Cells were resuspended in 300 µL PBS containing 4% paraformaldehyde for 1 h at room temperature. Cells were then washed with PBS and resuspended in 200 µL PBS. Fluorescence was measured at a fixed emission (670 nm) after excitation with a red laser (640 nm) using a Cytek Amnis CellStream flow cytometer (Cytek, Fremont, CA, USA) with 10,000 events per sample. No autofluorescence was observed.

RNA extraction

Mtb strains were grown in 10 mL square bottles in a shaking incubator at 37°C to reach OD_{600nm} ~ 0.8. Bacteria were harvested by centrifugation at 3,000 × *g* for 10 min at 4°C and washed once with cold sterile PBS. Total RNA was extracted using a FastRNA Pro Blue kit (MP) according to the manufacturer's instructions. The samples were treated with RNase-free DNase (Promega) for 3 h at 37°C to remove contamination of genomic DNA. The samples were purified with RNeasy columns (Qiagen) according to

Downloaded from https://journals.asm.org/journal/jb on 28 September 2026 by 2a0c:5bc0:40:1008:de4a:3eff:fe6a:56ad.

the manufacturer's instructions. The quantity and quality of RNA were assessed using a NanoDrop 1000 spectrophotometer (Thermo Fisher Scientific).

qRT-PCR

cDNA was produced from each RNA sample using the reverse transcriptase kit (Qiagen) as per the manufacturer's instructions. qRT-PCR was performed to quantify the expression levels of genes using the following primers: rv2702: forward primer, CCCT GGCTTAGTGGTACTGC; reverse primer, GTTGGGTATCAACGTCCCGT and rv0650: forward primer, CCTATCGACCTACACAGCGG; reverse primer, ACACCACCAAACCCAACAGA.

The expression levels of 16S rRNA were used as an internal control. Data were retrieved and processed with Microsoft Excel. The $\Delta\Delta_{CT}$ values were calculated for the genes to be tested in each sample using untreated bacteria as the control, and the fold changes of the expression levels were calculated as $2^{(-\Delta\Delta_{CT})}$.

Statistical analysis

The data are presented as the means ± SDs from two biological replicates and at least two technical replicates per condition. Unpaired two-tailed Student's *t*-tests were used to compare the data, and $P < 0.05$ was considered significant.

Biological safety considerations

The bacteria were handled within a Class-I safety-level cabinet in a containment level 3 laboratory.

ACKNOWLEDGMENTS

We would like to thank Dr. Sufyan Pandor and Dr. Hannah Florence from Agilent Technologies for the discussion and advice on the separation and detection of sugar monophosphate by LC/Q-TOF.

G.L-M. and B.D.R. received funding from the Medical Research Council MR/W018756/1. Metabolite identification work was supported by Dr. Elena Chekmeneva and Dr. Beatriz Jimenez of the National Phenome Centre. This work was supported by the Medical Research Council and the National Institute for Health Research (grant number MC_PC_12025). Infrastructure support was provided by the National Institute for Health Research (NIHR) Imperial Biomedical Research Centre (BRC).

Yi Liu: investigation, data analysis, visualization, and writing—original draft preparation; Nadine Ruecker: investigation, data analysis; Valwynne Faulker: investigation, data analysis, visualization; Kavitha Rachineni: investigation, data analysis, visualization; Nada Al-Saffar: investigation, data analysis, visualization; Elisabeth Oskoui: data analysis and editing; Larissa Zarate Garcia: data analysis and editing; Jessica Emma Rowley: data analysis and editing; Pablo Villacampa Teixeira: data analysis and editing; Tiago R. D. Costa: supervision and writing—review and editing; Eachan Johnson: supervision and writing—review and editing; Brian D. Robertson: investigation, funding acquisition, writing—review and editing; Sabine Ehrt: investigation, supervision, writing—review and editing; Gerald Larrouy-Maumus: conceptualization, funding acquisition, data analysis, supervision, writing—original draft preparation, and writing—review and editing. All authors have read and approved the manuscript.

AUTHOR AFFILIATIONS

[1]Department of Life Sciences, Faculty of Natural Sciences, Centre for Bacterial Resistance Biology, Imperial College London, London, United Kingdom
[2]Department of Microbiology and Immunology, Weill Cornell Medicine, New York, New York, USA
[3]Systems Chemical Biology of Infection and Resistance Laboratory, Francis Crick Institute, London, United Kingdom

Downloaded from https://journals.asm.org/journal/jb on 28 September 2026 by 2a0c:5bc0:40:1008:de4a:3eff:fe6a:56ad.

[4]Section of Bioanalytical Chemistry, Division of Systems Medicine, Department of Metabolism, Digestion and Reproduction, National Phenome Centre, Imperial College London, London, United Kingdom
[5]Flow Cytometry Facility, Department of Life Sciences, Faculty of Natural Sciences, Imperial College London, London, United Kingdom
[6]Department of Infectious Disease, Imperial College London, London, United Kingdom

AUTHOR ORCIDs

Eachan Johnson https://orcid.org/0000-0002-0335-8337
Sabine Ehrt https://orcid.org/0000-0002-7951-2310
Gerald Larrouy-Maumus http://orcid.org/0000-0001-6614-8698

FUNDING

Funder	Grant(s)	Author(s)
Medical Research Council	MC_PC_12025	Nada Al-Saffar
Medical Research Council	MR/W018756/1	Gerald Larrouy-Maumus

AUTHOR CONTRIBUTIONS

Yi Liu, Formal analysis, Investigation, Methodology | Nadine Ruecker, Formal analysis, Investigation | Valwynne Faulkner, Formal analysis, Investigation, Visualization | Kavitha Rachineni, Investigation, Methodology, Visualization | Nada Al-Saffar, Investigation, Methodology, Visualization | Elisabeth Oskoui, Methodology, Visualization | Larissa Zarate Garcia, Investigation, Methodology, Visualization | Jessica Emma Rowley, Investigation, Methodology, Visualization | Pablo Villacampa Teixeira, Investigation | Tiago R. D. Costa, Investigation | Eachan Johnson, Investigation, Methodology | Brian D. Robertson, Investigation | Sabine Ehrt, Investigation, Methodology.

DATA AVAILABILITY

All data presented in this study are contained within the article and available upon request from the corresponding author. The metabolomics data generated in this study have been deposited in the MetaboLights repository (28) with the study identifier MTBLS13438.

ADDITIONAL FILES

The following material is available online.

Supplemental Material

Supplemental material (JB00343-26-s0001.docx). Fig. S1 to S9; Tables S1 to S3.
Supplemental text (JB00343-26-s0002.docx). Supporting material.
Table S4 (JB00343-26-s0003.xlsx). Metabolites abundances batch corrected.

REFERENCES

1. WHO. 2022. Global tuberculosis report
2. Singh L, Karthikeyan S, Thakur KG. 2024. Biochemical and structural characterization reveals Rv3400 codes for β-phosphoglucomutase in *Mycobacterium tuberculosis*. Protein Sci 33:e4943. https://doi.org/10.1002/pro.4943
3. Barrozo A, Liao Q, Esguerra M, Marloie G, Florián J, Williams NH, Kamerlin SCL. 2018. Computer simulations of the catalytic mechanism of wild-type and mutant β-phosphoglucomutase. Org Biomol Chem 16:2060–2073. https://doi.org/10.1039/c8ob00312b
4. DeJesus MA, Gerrick ER, Xu W, Park SW, Long JE, Boutte CC, Rubin EJ, Schnappinger D, Ehrt S, Fortune SM, Sassetti CM, Ioerger TR. 2017. Comprehensive essentiality analysis of the *Mycobacterium tuberculosis* genome via saturating transposon mutagenesis. mBio 8:e02133-16. https://doi.org/10.1128/mBio.02133-16
5. Sassetti CM, Rubin EJ. 2003. Genetic requirements for mycobacterial survival during infection. Proc Natl Acad Sci USA 100:12989–12994. https://doi.org/10.1073/pnas.2134250100
6. Sassetti CM, Boyd DH, Rubin EJ. 2003. Genes required for mycobacterial growth defined by high density mutagenesis. Mol Microbiol 48:77–84. https://doi.org/10.1046/j.1365-2958.2003.03425.x
7. Joshi SM, Pandey AK, Capite N, Fortune SM, Rubin EJ, Sassetti CM. 2006. Characterization of mycobacterial virulence genes through genetic interaction mapping. Proc Natl Acad Sci USA 103:11760–11765. https://doi.org/10.1073/pnas.0603179103

Downloaded from https://journals.asm.org/journal/jb on 28 September 2026 by 2a0c:5bc0:40:1008:de4a:3eff:fe6a:56ad.

8. Elbein AD, Mitchell M. 1973. Levels of glycogen and trehalose in *Mycobacterium smegmatis* and the purification and properties of the glycogen synthetase. J Bacteriol 113:863–873. https://doi.org/10.1128/jb.113.2.863-873.1973
9. Winder FG, Tighe JJ, Brennan PJ. 1972. Turnover of acylglucose, acyltrehalose and free trehalose during growth of *Mycobacterium smegmatis* on glucose. J Gen Microbiol 73:539–546. https://doi.org/10.1099/00221287-73-3-539
10. Minnikin DE, Brennan PJ. 2020. Lipids of clinically significant mycobacteria, p 1–76. *In* Goldfine H (ed), Lipids of clinically significant mycobacteriahealth consequences of microbial interactions with hydrocarbons, oils, and lipids. Springer International Publishing, Cham.
11. Brennan PJ. 2003. Structure, function, and biogenesis of the cell wall of *Mycobacterium tuberculosis*. Tuberculosis (Edinb) 83:91–97. https://doi.org/10.1016/s1472-9792(02)00089-6
12. Brennan PJ, Nikaido H. 1995. The envelope of mycobacteria. Annu Rev Biochem 64:29–63. https://doi.org/10.1146/annurev.bi.64.070195.000333
13. Marrero J, Trujillo C, Rhee KY, Ehrt S. 2013. Glucose phosphorylation is required for *Mycobacterium tuberculosis* persistence in mice. PLoS Pathog 9:e1003116. https://doi.org/10.1371/journal.ppat.1003116
14. Kalscheuer R, Weinrick B, Veeraraghavan U, Besra GS, Jacobs WR Jr. 2010. Trehalose-recycling ABC transporter LpqY-SugA-SugB-SugC is essential for virulence of *Mycobacterium tuberculosis*. Proc Natl Acad Sci USA 107:21761–21766. https://doi.org/10.1073/pnas.1014642108
15. Furze CM, Delso I, Casal E, Guy CS, Seddon C, Brown CM, Parker HL, Radhakrishnan A, Pacheco-Gomez R, Stansfeld PJ, Angulo J, Cameron AD, Fullam E. 2021. Structural basis of trehalose recognition by the mycobacterial LpqY-SugABC transporter. J Biol Chem 296:100307. https://doi.org/10.1016/j.jbc.2021.100307
16. Reyes AM, Pedre B, De Armas MI, Tossounian M-A, Radi R, Messens J, Trujillo M. 2018. Chemistry and redox biology of mycothiol. Antioxid Redox Signal 28:487–504. https://doi.org/10.1089/ars.2017.7074
17. Cumming BM, Chinta KC, Reddy VP, Steyn AJC. 2018. Role of ergothioneine in microbial physiology and pathogenesis. Antioxid Redox Signal 28:431–444. https://doi.org/10.1089/ars.2017.7300
18. Sao Emani C, Williams MJ, Van Helden PD, Taylor MJC, Wiid IJ, Baker B. 2018. Gamma-glutamylcysteine protects ergothioneine-deficient *Mycobacterium tuberculosis* mutants against oxidative and nitrosative stress. Biochem Biophys Res Commun 495:174–178. https://doi.org/10.1016/j.bbrc.2017.10.163
19. Saini V, Cumming BM, Guidry L, Lamprecht DA, Adamson JH, Reddy VP, Chinta KC, Mazorodze JH, Glasgow JN, Richard-Greenblatt M, Gomez-Velasco A, Bach H, Av-Gay Y, Eoh H, Rhee K, Steyn AJC. 2016. Ergothioneine maintains redox and bioenergetic homeostasis essential for drug susceptibility and virulence of *Mycobacterium tuberculosis*. Cell Rep 14:572–585. https://doi.org/10.1016/j.celrep.2015.12.056
20. Richard-Greenblatt M, Bach H, Adamson J, Peña-Diaz S, Li W, Steyn AJC, Av-Gay Y. 2015. Regulation of ergothioneine biosynthesis and its effect on *Mycobacterium tuberculosis* growth and infectivity. J Biol Chem 290:23064–23076. https://doi.org/10.1074/jbc.M115.648642
21. Kalera K, Liu R, Lim J, Pathirage R, Swanson DH, Johnson UG, Stothard AI, Lee JJ, Poston AW, Woodruff PJ, Ronning DR, Eoh H, Swarts BM. 2024. Targeting *Mycobacterium tuberculosis* persistence through inhibition of the trehalose catalytic shift. ACS Infect Dis 10:1391–1404. https://doi.org/10.1021/acsinfecdis.4c00138
22. Lee JJ, Swanson DH, Lee S-K, Dihardjo S, Lee GY, Gelle S, Seong HJ, Bravo ERM, Taylor ZE, Van Nieuwenhze MS, Singh A, Lee J-S, Eum S, Cho S, Swarts BM, Eoh H. 2025. Trehalose catalytic shift inherently enhances phenotypic heterogeneity and multidrug resistance in *Mycobacterium tuberculosis*. Nat Commun 16:6442. https://doi.org/10.1038/s41467-025-61703-3
23. Gee CL, Papavinasasundaram KG, Blair SR, Baer CE, Falick AM, King DS, Griffin JE, Venghatakrishnan H, Zukauskas A, Wei J-R, Dhiman RK, Crick DC, Rubin EJ, Sassetti CM, Alber T. 2012. A phosphorylated pseudokinase complex controls cell wall synthesis in mycobacteria. Sci Signal 5:ra7. https://doi.org/10.1126/scisignal.2002525
24. Stover CK, de la Cruz VF, Fuerst TR, Burlein JE, Benson LA, Bennett LT, Bansal GP, Young JF, Lee MH, Hatfull GF, Snapper SB, Barletta RG, Jacobs WR Jr, Bloom BR. 1991. New use of BCG for recombinant vaccines. Nature 351:456–460. https://doi.org/10.1038/351456a0
25. Nandakumar M, Prosser GA, de Carvalho LPS, Rhee K. 2015. Metabolomics of *Mycobacterium tuberculosis*. Methods Mol Biol 1285:105–115. https://doi.org/10.1007/978-1-4939-2450-9_6
26. de Carvalho LPS, Fischer SM, Marrero J, Nathan C, Ehrt S, Rhee KY. 2010. Metabolomics of *Mycobacterium tuberculosis* reveals compartmentalized co-catabolism of carbon substrates. Chem Biol 17:1122–1131. https://doi.org/10.1016/j.chembiol.2010.08.009
27. Dona AC, Jiménez B, Schäfer H, Humpfer E, Spraul M, Lewis MR, Pearce JTM, Holmes E, Lindon JC, Nicholson JK. 2014. Precision high-throughput proton NMR spectroscopy of human urine, serum, and plasma for large-scale metabolic phenotyping. Anal Chem 86:9887–9894. https://doi.org/10.1021/ac5025039
28. Yurekten O, Payne T, Tejera N, Amaladoss FX, Martin C, Williams M, O'Donovan C. 2024. MetaboLights: open data repository for metabolomics. Nucleic Acids Res 52:D640–D646. https://doi.org/10.1093/nar/gkad1045

Downloaded from https://journals.asm.org/journal/jb on 28 September 2026 by 2a0c:5bc0:40:1008:de4a:3eff:fe6a:56ad.